

Optical phonon modes in LaInO_3 : Lattice dynamics and complete polarization analysis of Raman-active modes

H. Tornatzky¹, Z. Galazka², R. Gillen³, O. Brandt¹, M. Ramsteiner¹, M. R. Wagner¹

¹ Paul-Drude-Institute for Solid State Electronics, Hausvogteiplatz 5–7, 10117 Berlin
Germany

² Leibniz-Institut für Crystal Growth, Max-Born-Str. 2, 12489 Berlin, Germany

³ Friedrich-Alexander University Erlangen-Nuremberg, Staudtstrasse 7, 91058 Erlangen,
Germany

LaInO_3 is part of the family of ABO_3 perovskites, and is considered promising for next generation devices, such as for power electronics, due to its band gap of about 4.5 eV. A detailed knowledge of phonon modes in LaInO_3 is important as they determine a number of material properties, such as the mechanical and elastic properties, thermal transport and carrier dynamics, phonon-assisted optical excitations, and many more. However, little is known about the vibrational properties of this material. In this study, we investigate the lattice dynamics by polarization- and angle-resolved Raman spectroscopy and density functional theory (DFT). We experimentally observe all but one of the Raman active modes and compare them to our simulated values from DFT. Furthermore, we present the DFT-derived phonon dispersion relation along the high symmetry directions in reciprocal space and depict the oscillation patterns for selected phonons at the Γ point. Finally, we determine the relative Raman tensor elements of the observed modes from the angular dependence of their corresponding scattering efficiencies (cf. Fig. 2).

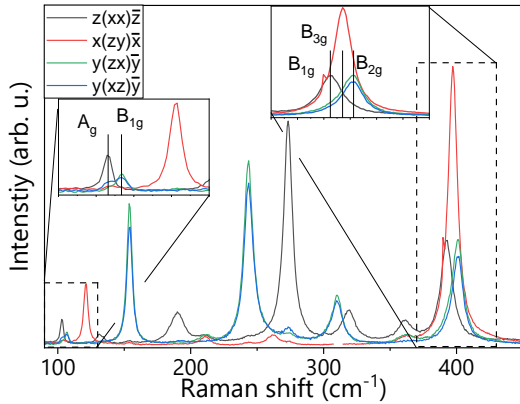


Figure 1: Polarized Raman spectra allow to distinguish overlapping modes based on their symmetry (see insets).

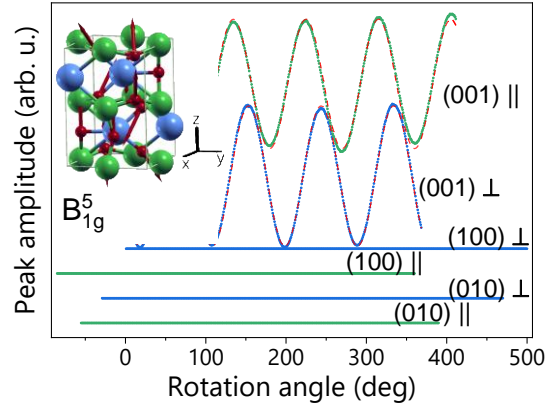


Figure 2: Angle resolved peak amplitude of the B_{1g}^5 mode for different scattering configurations (vertically offset). Blue and green symbols depict the measurement, red dashed lines depict the fit.

⁺ Author for correspondence: Tornatzky@PDI-Berlin.de

Supplementary Pages

Figure 3 shows the polarized Raman spectra on the (100), (010) and (100) faces of macroscopic melt-grown crystals. The coordinate system xyz is chosen to be parallel to the a , b and c lattice vectors. By careful analysis of the polarization resolved spectra, one can identify 23 of the 24 active Raman modes, of which many overlap and are indistinguishable in unpolarized measurements. The positions of all observed modes are indicated by vertical dashed lines in Fig. 3. The remaining mode is expected to be either obscured by a mode of the same symmetry or very weak in intensity.

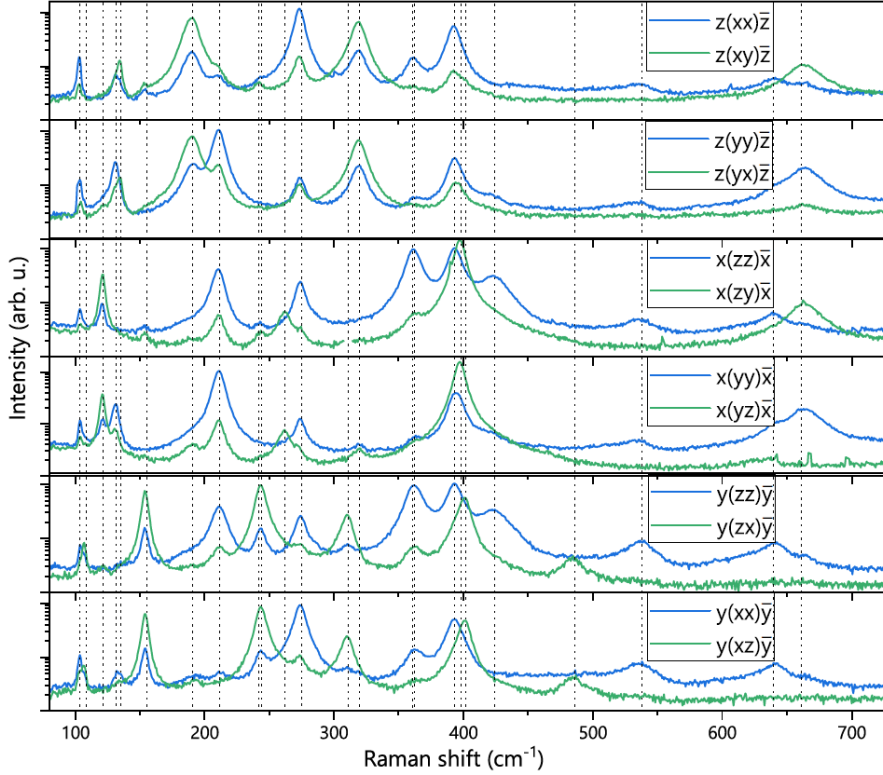


Figure 3: Polarization-resolved Raman spectra of LaInO_3 with scattering direction and polarization parallel to the lattice vectors (scattering geometry is given in Porto notation). Vertical dashed lines indicate the position of observed Raman active phonon modes.

DFT as implemented in the Quantum Espresso-suite [1] was used with Perdew-Burke-Ernzerhof functionals to calculate the phonon dispersion and derive the oscillation patterns of the phonon modes at the Γ point. Norm conserving ultra-soft pseudopotentials were used with a kinetic cutoff-energy of 80 Ry (800 Ry) for the wave function (charge density and potential). Both, electronic and vibrational properties were calculated on a regular $6 \times 6 \times 4$ k/q -grid pattern. The obtained lattice parameters of $a = 5.776 \text{ \AA}$, $b = 6.015 \text{ \AA}$ and $c = 8.348 \text{ \AA}$ are in good agreement with values measured by x-ray diffraction. Figure 4 shows the obtained phonon dispersion along the high-symmetry path $\Gamma\text{XSY}\Gamma\text{ZURTZ|UX|SR|YT}$ (cf. inset). The obtained phonon energies are generally in good agreement with the experiment, but deviate for some modes, especially for the high frequency modes. This deviation is considered as an effect of a nonideal oxygen pseudopotential. The results from DFT further suggest that the final mode to be observed experimentally is the B_{3g}^3 mode which is nearly degenerate with the A_g^6 mode. Further analysis of the data will be needed to potentially distinguish these two lines. The phonon density of states has been calculated on a regular $50 \times 50 \times 50$ q -point grid and is depicted in the right panel of Fig. 4.

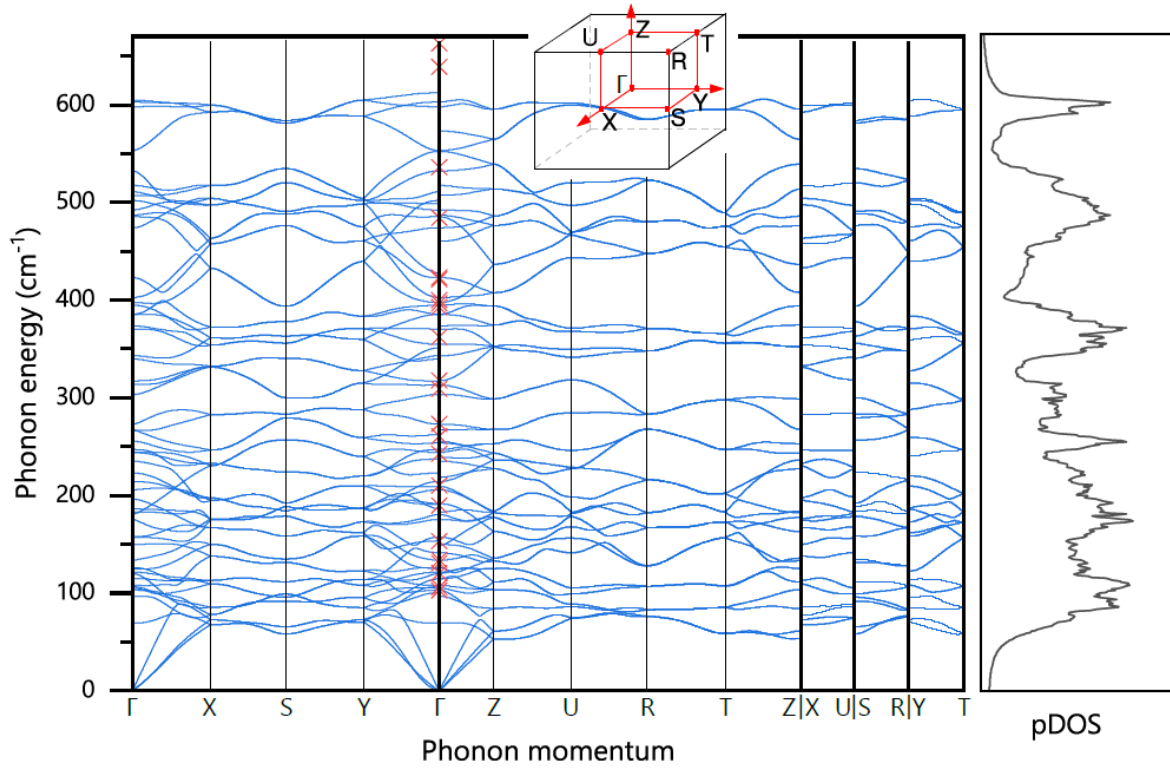


Figure 4: Phonon dispersion of LaInO_3 . Lines (symbols) represent the simulation (experiment). The inset depicts the Brillouin zone with its high symmetry points. The right panel shows the phonon density of states (pDOS).

Our angular resolved Raman measurements allow us to analyze the Raman scattering efficiency for arbitrary polarization configurations. Figure 2 shows the evolution of the amplitude of the B_{1g}^5 mode at 319 cm^{-1} , with the rotation angle on the different crystal faces. The fit function can be calculated from the well-known relation of the intensity with the scattering geometry and the Raman tensor $I \propto |e_i R e_s|^2$, where R is the Raman tensor of the mode and e_i and e_s are the polarization of the incident and scattered light. The latter can be parameterized, such as $e_i, e_s = (\sin(\phi), \cos(\phi), 0)$, to describe the angular dependence. The angular dependence on the (001) plane is then calculated as $d^2 \sin^2(2\phi)$ and $d^2 \cos^2(2\phi)$ for parallel and crossed polarization. Fitting all angular profiles of one mode, with common parameters, allows the experimental determination of the relative Raman tensor elements.

All in all, we have analyzed the vibrational properties in LaInO_3 both experimentally and theoretically. We were able to observe most of the Raman active modes and measure their angular dependent scattering behavior, which allowed us to extract the relative Raman tensor elements. Our theoretical simulations are in good agreement with our experimental results and make oscillation patterns of the different modes available. These results provide the basis for a better understanding of the growth of LaInO_3 by the possibility to link changes in growth to the changes in the lattice (mechanical strain, alloying, phase coexistence, etc.), it allows better theoretical prediction of properties such as heat transport in devices, and it provides the necessary input for understanding phonon-mediated optical processes.